

# Electromagnetic signatures of white dwarf collisions in AGN discs

Shu-Rui Zhang,<sup>1,2\*</sup> Yan Luo,<sup>1,2</sup> Xiao-Jun Wu,<sup>1,2</sup> Jian-Min Wang,<sup>3</sup> Luis C. Ho,<sup>4,5</sup> Ye-Fei Yuan<sup>1,2 †</sup>

<sup>1</sup>*School of Astronomy and Space Science, University of Science and Technology of China, Hefei 230026, China*

<sup>2</sup>*CAS Key Laboratory for Research in Galaxies and Cosmology, Department of Astronomy, University of Science and Technology of China, Hefei 230026, China*

<sup>3</sup>*Key Laboratory for Particle Astrophysics, Institute of High Energy Physics, Chinese Academy of Sciences, 19B Yuquan Road, Beijing 100049, China*

<sup>4</sup>*Kavli Institute for Astronomy and Astrophysics, Peking University, Beijing 100871, China*

<sup>5</sup>*Department of Astronomy, School of Physics, Peking University, Beijing 100871, China*

Accepted 2023 June 15. Received 2023 June 15; in original form 2022 September 30

## ABSTRACT

In the inner region of the disc of an active galactic nucleus (AGN), the collision of two white dwarfs (WDs) through Jacobi capture might be inevitable, leading to a Type Ia supernova (SN Ia) explosion. This transient event, influenced by the disc gas and the gravity of the supermassive black hole (SMBH), exhibits distinct characteristics compared to normal SNe Ia. The energy of the explosion is mainly stored in the ejecta in the form of kinetic energy. Typically, the ejecta is not effectively decelerated by the AGN disc and rushes rapidly out of the AGN disc. However, under the influence of the SMBH, most of the ejecta falls back toward the AGN disc. As the fallback ejecta becomes more dispersed, it interacts with the disc gas, converting its kinetic energy into thermal energy. This results in a high-energy transient characterized by a rapid initial rise followed by a decay with  $L \propto t^{-2.8}$ . The time-scale of the transient ranges from hours to weeks, depending on the mass of the SMBH. This process generates high-energy radiation spanning from hard X-rays to the soft  $\gamma$  range. Additionally, the subsequent damage to the disc may result in changing-look AGNs. Moreover, the falling back of SNe Ia ejecta onto the AGN disc significantly increases the metallicity of the AGN and can even generate heavy elements within the AGN discs.

**Key words:** accretion, accretion discs – binaries: general – white dwarfs – quasars: supermassive black holes – gamma-rays: general – transients: supernovae

## 1 INTRODUCTION

Compact objects, including white dwarfs (WDs), are believed to exist in the accretion discs of active galactic nuclei (AGN; Ostriker 1983; McKernan et al. 2012; McKernan et al. 2020; Zhu et al. 2021b), with a predicted high rate of WD-WD mergers (McKernan et al. 2020). However, the specific mechanisms governing the interaction among WDs in AGN discs and the potential observational phenomena remain unclear. From an observational perspective, phenomena such as AGN variations (e.g. Gopal-Krishna et al. 2019), changing-look AGNs (e.g. Ricci et al. 2020; Trakhtenbrot et al. 2019), and the super-solar metallicity of quasars (Warner et al. 2003; Nagao et al. 2006; Shin et al. 2013; Du et al. 2014; Maiolino & Mannucci 2019) still lack complete understanding. Longstanding issues include the mechanisms by which the extreme environments of AGNs supply and transfer energy, as well as the production of heavy elements in these surroundings.

Numerous physical processes involving compact objects have been proposed within AGN discs (e.g., Cheng & Wang 1999; Wang et al. 2021a,b; Tagawa et al. 2020). Bound stars around supermassive black hole (SMBHs) can originate from nuclear star clusters (Tagawa et al. 2020). The SMBH can capture stars through either tidal breakup of binary systems (for SMBHs with masses  $M_{\text{SMBH}} \sim 10^6 M_{\odot}$ ) or suc-

cessive dissipative encounters with the disc (for  $M_{\text{SMBH}} \sim 10^8 M_{\odot}$ ; Syer et al. 1991). These bound stars (or compact objects formed through evolution) interact continuously with the AGN disc, facilitating the exchange of angular momentum and energy between the compact objects and the disc (Ostriker 1983). Consequently, the orbits of compact objects are confined to the disc (Fabj et al. 2020; Yang et al. 2019b; Bartos et al. 2017; Tanaka et al. 2002). Furthermore, stars can form in the outer region of the AGN disc ( $\gtrsim 10^4 r_g$ , where  $r_g$  is defined as  $GM_{\text{SMBH}}/c^2$ , and  $c$  is the speed of light) due to gravitational instability and subsequently evolve into compact objects (Stone et al. 2017; Dittmann & Miller 2020; Derdzinski & Mayer 2022). The orbits of these compact objects within the AGN disc are influenced by the gravity of the SMBH and the presence of disc gas, causing the objects to migrate inward towards migration traps (Bellovary et al. 2016) or regions with varying aspect ratios (McKernan et al. 2014). Consequently, various processes, including accumulation, accretion growth, collision, and scattering of compact objects, occur within these regions (e.g., Tagawa et al. 2020; Yang et al. 2019a; Secunda et al. 2019; Gayathri et al. 2020; Vijaykumar et al. 2022). Notably, Samsing et al. (2022) conducted a study on the three-body interactions of black holes (BHs) within AGN discs, revealing that AGN discs can lead to binary mergers with high eccentricities. Additionally, Wang et al. (2021b); Rowan et al. (2022); Kaaz et al. (2021) proposed that compact objects within AGN discs can capture one another, forming binaries and generating multi-band electromagnetic and gravitational wave (GW) radiation. Further re-

\* E-mail: zhangsr@mail.ustc.edu.cn (SRZ)

† E-mail: yfyuan@ustc.edu.cn (YFY)

search by [Li et al. \(2022b\)](#) and [Boekholt et al. \(2023\)](#) demonstrated that Jacobi capture in the disc can result in the formation of eccentric BH binaries, which subsequently merge within a few binary orbits.

The evolution of WDs and their binaries in AGN discs is expected to differ from that of BHs. This difference can be attributed, at least in part, to the larger radii of WDs. Furthermore, AGN discs are anticipated to contain a higher number of WDs compared to BHs, as the number density of WDs is higher ([Kroupa 2001](#)), although the mass function of stars in AGN discs tends to be "top heavy" ([Derdzinski & Mayer 2022](#)). Moreover, WDs in AGN discs do not easily reach the Chandrasekhar limit through accretion ([Pan & Yang 2021b](#)). Therefore, it is expected that two-body or multi-body interactions involving WDs would occur within the AGN disc. Specifically, Jacobi capture is a mechanism that allows two WDs to collide directly instead of forming a WD binary ([Luo et al. 2023](#)). Collisions between two WDs are considered as one of the possible pathways for the formation of SNe Ia ([Rosswog et al. 2009](#); [Raskin et al. 2009](#); [Hawley et al. 2012](#)). Although SNe Ia have been utilized as standard candles for measuring the accelerated expansion of the universe ([Riess et al. 1998](#); [Schmidt et al. 1998](#); [Perlmutter et al. 1999](#)), their progenitor systems (e.g., [Whelan & Iben 1973](#); [Hoyle & Fowler 1960](#); [Webbink 1984](#); [Taam 1980](#); [Rosswog et al. 2009](#); [Raskin et al. 2009](#); [Wang & Han 2012](#)) and explosion mechanisms are still subject to controversy (e.g., [Hillebrandt et al. 2013](#); [Maoz et al. 2014](#); [McCutcheon et al. 2022](#)). Theoretical models, simulations (e.g., [Mazzali et al. 2001](#); [Iwamoto & Kunugise 2006](#); [Rosswog et al. 2009](#); [Raskin et al. 2009](#)), and observations ([Hayden et al. 2010](#)) of SNe Ia suggest that only a small fraction of the explosion energy is converted into neutrinos and electromagnetic radiation, while the majority is in the form of kinetic energy. The environment of the AGN disc, characterized by the gravity of the SMBH and high-density gas, can effectively harness the kinetic energy of the ejecta. The disc gas efficiently converts the kinetic energy into electromagnetic radiation, which serves as a potential power source for electromagnetic transient. Additionally, the initial explosion and fallback ejecta may cause disturbances or disruptions in the disc, potentially resulting in observable phenomena.

To date, research on WD explosions in AGN discs has only focused on the interactions between the supernova explosion and the gas of AGN discs during the early phase of evolution. [Rozyczka et al. \(1995\)](#); [Moranchel-Basurto et al. \(2021\)](#) have studied the effects of supernova explosions in the outer region of an accretion disc ( $\sim 10^4 r_g$ ), around a relative massive SMBH ( $M_{\text{SMBH}} \gtrsim 10^8 M_\odot$ ). They found that the explosions do not disrupt the disc, but can induce substantial angular momentum redistribution. [Perna et al. \(2021\)](#) have studied relativistic explosions in AGN discs and extended the standard internal/external shock model ([Rees & Meszaros 1994](#); [Piran 1999](#); [Mészáros & Rees 1997](#)) to the AGN disc environment. [Zhu et al. \(2021b\)](#) studied thermonuclear explosions and accretion-induced collapse of WDs in AGN discs, but [Pan & Yang \(2021b\)](#) shows that WD should not be able to reach the Chandrasekhar limit through accretion. The AGN disc considered is thick and the explosive ejecta can slow down effectively, but the shock wave can explode on the surface of the AGN disc. These processes are verified by numerical simulations that assume that the explosion is located in the region  $10^3 \sim 10^4 r_g$  ([Grishin et al. 2021](#)). The previous studies either made assumptions about explosions occurring within a specific radius range or focused on analyzing thick discs. However, they did not examine the potential consequences of failing to dissipate the immense kinetic energy generated by the explosion fully. Actually, the location of migration traps is usually  $\lesssim 10^3 r_g$  if it exists ([Bellovary et al. 2016](#); [Derdzinski & Mayer 2022](#)), and the innermost migration

trap can even reach the innermost circular orbit ([Peng & Chen 2021](#)). In addition to a migration trap, an overdensity of compact objects within the disc can also arise in regions where there are changes in the aspect ratio or migration time-scale ([McKernan et al. 2014](#)). According to [McKernan et al. \(2012\)](#), the migration timescale of  $1 - M_\odot$  compact stars also increases inwards at  $\lesssim 10^3 r_g$ . At this location, the gas of the AGN disc is not thick enough, and the explosion ejecta is usually not decelerated effectively. Thus, the ejecta can rush out of the AGN disc. Under the dominance of SMBH gravity, part of the ejecta can fall back on to the AGN disc. As the dispersed ejecta falls towards the AGN disc, its interaction with the disc results in the conversion of kinetic energy, leading to the production of high-temperature plasma on the surface of the disc.

In this work, we investigate the collision of two WDs leading to a SN Ia explosion through Jacobi capture within the inner region of the AGN disc, and the following observable consequences arising after the interaction between the fallback ejecta of the explosion and the AGN disc. Our results show the potential connection between this event and various phenomena observed in AGNs, including AGN variations, changing-look AGNs, and the presence of supersolar metallicity in AGNs. The introduction of our model is presented in Section 2. The light curves generated from the fallback ejecta hitting the AGN disc are shown in Section 3, and the spectral energy distribution (SED) is provided in Section 4, demonstrating the potential for high-energy radiation generation. The main results, model uncertainties and potential implications are discussed in Section 5. Lastly, the main conclusions are summarized in Section 6.

## 2 THEORETICAL MODEL

In this section, we provide a comprehensive description of the explosion model resulting from the collision of two WDs within an AGN disc. Although the primary objective of this model is to address the explosion caused by the collision of two WDs within an AGN disc, it can be applied to other explosive events occurring within AGN discs, which also involve the fallback of ejecta.

### 2.1 WD-WD close encounters in AGN discs

Our discussion here is based on the model of [Li et al. \(2022b\)](#) and [Boekholt et al. \(2023\)](#), who discuss the close encounter between two stellar massive BHs in an AGN disc. One can also find recent modeling work including gas effects ([Rowan et al. 2022](#)). In the AGN disc, the rate of the close encounter between stellar massive BHs will be enhanced in regions with migration traps or varying aspect ratios, but the relative kinetic energy of two encountering BHs is usually too large to form bound binary BHs. In order to form a bound binary BH, a very close encounter is required, so that the gravitational wave radiation is strong enough to carry away the excess relative kinetic energy. Similar to the qualitative analysis in [Li et al. \(2022b\)](#), we examine the close encounter of two WDs in an AGN disc. To ensure comprehensiveness, we provide only the necessary analysis; detailed information can be found in [Luo et al. \(2023\)](#).

Let us consider a SMBH mass of  $M_{\text{SMBH}} \sim 10^7 M_\odot$  and two identical WDs that are almost coplanar in a circular orbit in an AGN disc. The semi-major axes of the two WDs around the SMBH are  $a_1 \approx a_2 \sim 100 r_g \approx 1.5 \times 10^9$  km. Suppose that the masses and radii of the two WDs are  $m_1 = m_2 = 1.0 M_\odot$  and  $R_{\text{WD}} \sim 10^4$  km, respectively. Then the mutual Hill radius between the two WDs is given by

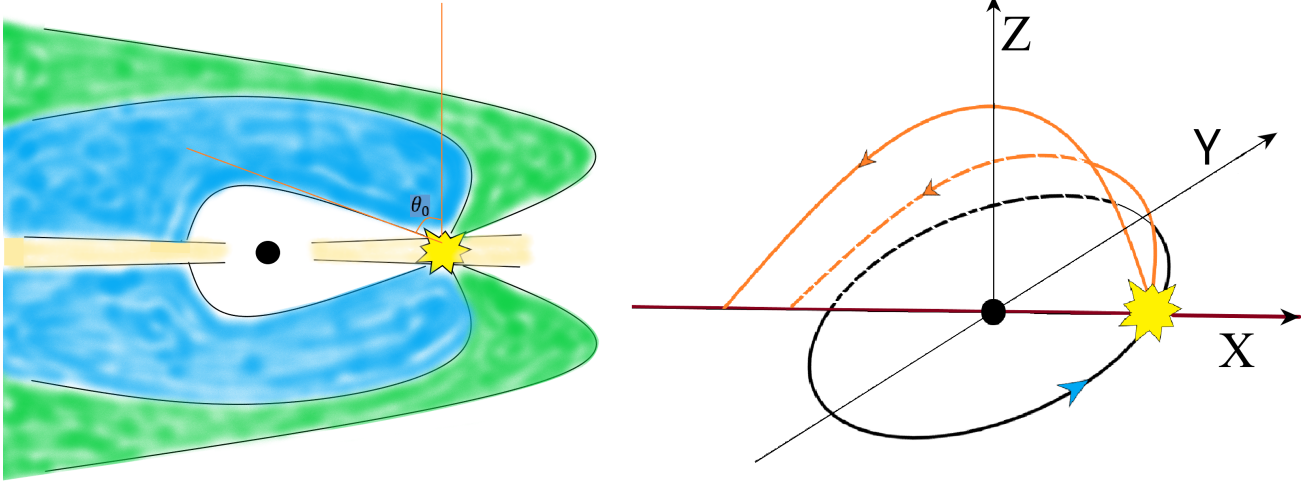


**Figure 1.** Schematic illustration of WD-WD collision in an AGN disc. **Left panel:** The collision between two WDs leads to a SN Ia explosion. Subsequently, the ejected material escapes rapidly from the AGN disc. Due to the gravitational pull of the SMBH, a significant portion of the ejecta falls back onto the AGN disc, while some parts manage to escape the system. In our model, we assume that the ejecta with launch angles  $\theta < \theta_0 = 89^\circ$  can successfully escape the disc. The unbound material is depicted in green, whereas the bound material is shown in blue, representing the material that can fall back to the AGN disc. **Right panel:** Schematic representation of the coordinate system employed in the description. The black ellipse in the coordinate system corresponds to the trajectory of the center of mass of the two WDs before the collision. The X-axis is defined as the line along the collision point and the SMBH. The trajectory of the ejecta following the explosion is represented by the orange line. The points where the ejected material can fall back onto the AGN disc are positioned along the X-axis.

$$R_H \equiv \frac{a_1 + a_2}{2} \left( \frac{m_1 + m_2}{3M_{\text{SMBH}}} \right)^{\frac{1}{3}} \approx 4 \times 10^{-3} a_1 \approx 6 \times 10^6 \text{ km}. \quad (1)$$

If the orbital separation of the two WDs is less than  $2\sqrt{3}R_H$  (Gladman 1993), the orbits are dynamically unstable. In order to have two unstable WDs captured into a bound binary, GW emission must be dominant, which means that the energy loss by GW emission should follow (Li et al. 2022b)

$$\Delta E_{\text{GW}} \gtrsim \zeta \frac{Gm_1m_2}{R_H}, \quad (2)$$

with  $\zeta$  of order unity. Setting the distance at close encounter as  $R_{\text{cap}}$ ,

$$\frac{R_{\text{cap}}}{R_H} \approx 10^{-4}. \quad (3)$$

Thus,  $R_{\text{cap}} \approx 600$  km. It should be noted that  $R_{\text{cap}} \approx 600$  km is much smaller than a typical WD radius of  $R_{\text{WD}} \sim 10^4$  km. This indicates that the two WDs collide before a bound binary is formed. In a WD,  $mV$  is a constant, where  $m$  is the mass and  $V$  is the volume of the WD. Namely, the larger the radius of a WD, the easier it is for two WDs to collide instead of forming a binary. Thus, taking the above typical values is reasonable.

The collision of two WDs may produce SNe Ia (Rosswog et al. 2009; Raskin et al. 2009; Hawley et al. 2012). It is worth noting again that WDs in AGN disc are hard to grow to the Chandrasekhar limit through accretion, because WDs can be spun up more efficiently to reach the shedding limit (Pan & Yang 2021b). This implies that SNe Ia in AGN disc may form mainly by collisions of two WDs rather than through the single-degenerate or usual binary merger channels.

## 2.2 The supernova ejecta rushes out of AGN discs

Usually, the total energy from a SN Ia explosion is  $\sim 1.5 \times 10^{51}$  erg, of which the amount taken away by neutrinos is  $\sim 10^{50}$  erg and

that by electromagnetic radiation is  $\sim 10^{49}$  erg (Mazzali et al. 2001; Iwamoto & Kunugise 2006; Hayden et al. 2010). Consequently, the majority of the total energy is converted into kinetic energy of the ejecta, leaving only a small fraction of the energy taken away by neutrinos and electromagnetic radiation. Several studies (Rosswog et al. 2009; Raskin et al. 2009; Hawley et al. 2012) have simulated SNe Ia resulting from the collision of two WDs. The nuclear detonation triggered by the collision leads to a homologous explosion with velocities ranging from  $1.3 \times 10^4$  to  $1.6 \times 10^4$  km s $^{-1}$ , corresponding to a kinetic energy of approximately  $10^{51}$  erg. The resulting electromagnetic radiation is similar to that observed in normal SNe Ia.

By taking into account the collision of two WDs within the gaseous environment of an AGN disc and the subsequent supernova explosion, it becomes feasible to calculate the mass that is swept by the ejected material within the AGN disc. We choose the standard disc model of Kato et al. (2008) to describe the AGN disc. This disc model, which covers our regions of interest ( $\lesssim 10^3 r_g$ ), is akin to the one described in Sirko & Goodman (2003). The parameters chosen in our computations include an accretion rate of  $\dot{M} = 0.1 \dot{M}_{\text{Edd}}$  and a viscosity of  $\alpha = 0.1$ , where  $\dot{M}_{\text{Edd}}$  represents the Eddington rate. The scale height and density in the models are kept as continuous. Table 1 displays the disc mass swept by the ejecta for the different central SMBH masses and explosion radii. It can be seen that, in our intriguing cases of explosion in AGN discs (i.e.  $M_{\text{SMBH}} \lesssim 10^8 M_\odot$ , explosion radius  $R_{\text{ej}} \lesssim 10^3 r_g$ ), the swept mass is much less than the mass of the explosive ejecta ( $\sim 1 M_\odot$ ). It is noted that in the other AGN disc models (e.g. Thompson et al. 2005) the amounts of the swept-up disc gas is even lower.

Apparently, the AGN disc gas is too thin (i.e. the value of  $\rho \times H^3$  is too small, where  $\rho$  is the density in the disc midplane and  $H$  is the disc scale height, but the disc is still optically thick) for ejecta to slow down effectively. Locally, the ejecta inevitably rushes out of the AGN disc at nearly the initial explosion velocity. At a distance of  $\sim 100 r_g$ , the escape velocity is  $v_{\text{esc}} \sim 3\sqrt{2} \times 10^4$  km s $^{-1}$ . The ejecta that rushes

**Table 1.** The mass of disc gas swept by ejecta as it rushes out of the disc. It is assumed that the explosions occur in the midplane of the AGN disc. The AGN disc model is taken from the standard disc model of [Kato et al. \(2008\)](#).

$M_{\text{SMBH}} = 10^6 M_{\odot}, \dot{M} = 0.1 \dot{M}_{\text{Edd}}, \alpha = 0.1$			
Explosion radius ( $r_{\text{g}}$ )	100	200	500
Swept disc mass (g)	$2.51 \times 10^{27}$	$7.78 \times 10^{27}$	$3.31 \times 10^{28}$
$M_{\text{SMBH}} = 10^7 M_{\odot}, \dot{M} = 0.1 \dot{M}_{\text{Edd}}, \alpha = 0.1$			
Explosion radius ( $r_{\text{g}}$ )	100	200	500
Swept disc mass (g)	$2.51 \times 10^{29}$	$7.78 \times 10^{29}$	$3.31 \times 10^{30}$
$M_{\text{SMBH}} = 10^8 M_{\odot}, \dot{M} = 0.1 \dot{M}_{\text{Edd}}, \alpha = 0.1$			
Explosion radius ( $r_{\text{g}}$ )	100	200	500
Swept disc mass (g)	$2.51 \times 10^{31}$	$7.78 \times 10^{31}$	$3.31 \times 10^{32}$

out of the AGN disc is subject to the gravitational influence of the SMBH, resulting in some of it falling back towards the AGN disc, while other parts may escape from the system. Therefore, several observational effects can be anticipated: (i) the initial explosion is similar to that of a normal SN Ia, being powered by radioactivity decay and peaking in optical band ([Pereira et al. 2013](#)); (ii) the collision between the fallback ejecta and the AGN disc can give rise to the emergence of hard X-ray and soft gamma-ray transients. (iii) the destruction of the AGN disc by the fallback ejecta results in a temporary increase, then decrease, and finally a return to normal levels again in the accretion rate and luminosity ([McKernan et al. 2022](#)), similar to the observed changing-look AGN ([Ricci et al. 2020](#); [Trakhtenbrot et al. 2019](#); [Li et al. 2022a](#)).

The collisions between the fallback ejecta and the AGN disc, in conjunction with the supernova explosions of the WD system, give rise to significant new features. In the subsequent section, a model is constructed to explore the observational consequences resulting from these interactions (ii). The effects of (i) and (iii) will be discussed in detail in the Discussion section.

### 2.3 Fallback model

As shown in Fig. 1, it is assumed that the supernova explosion occurs in the midplane of the disc, resulting in symmetric motion of the ejecta about the disc plane. When two WDs collide, the center of mass moves in a circular Keplerian orbit around the SMBH. Following the triggered nuclear detonation after the collision, the ejecta undergoes homologous expansion with a typical velocity of  $1.5 \times 10^4 \text{ km s}^{-1}$ . Subsequent to the supernova explosion, the ejecta is propelled out of the AGN disc at nearly its initial velocity. Under the influence of the SMBH gravity, certain portions of the ejecta fall back along the negative X-axis of the disc, while other portions escape from the system. The focus of interest lies in the radiation generated by the interaction between the fallback ejecta and the disc. A typical explosion radius of  $\sim 100r_{\text{g}}$  is assumed, and Newtonian gravity is employed. It is worth noting that if the ejecta has the potential to fall back, the fallback points are situated on the X-axis, as depicted in the right panel of Fig. 1. Furthermore, even some components of gravitationally unbound ejecta can fall back to the disc if their hyperbolic trajectory intersects the disc.

Specifically, in our model the ejecta is assumed to be distributed spherically symmetrically at the explosion point. The ejecta is divided into  $N$  parts, with  $N = 2 \times 10^5$ . Monte Carlo simulations are conducted to determine the polar angle and azimuth angle of the

**Table 2.** Ratio of fallback ejecta with different model parameters. The columns from left to right in the table represent the mass of the SMBH, explosion radius, explosion velocity, the corresponding ratio of fallback ejecta.

$M_{\text{SMBH}}$	$R_{\text{ej}}$	$v_{\text{ej}}$	Ratio
$10^6 M_{\odot}$	$100r_{\text{g}}$	$1.5 \times 10^4 \text{ km s}^{-1}$	0.8873
$10^6 M_{\odot}$	$200r_{\text{g}}$	$1.5 \times 10^4 \text{ km s}^{-1}$	0.7107
$10^6 M_{\odot}$	$300r_{\text{g}}$	$1.5 \times 10^4 \text{ km s}^{-1}$	0.6204
$10^6 M_{\odot}$	$500r_{\text{g}}$	$1.5 \times 10^4 \text{ km s}^{-1}$	0.5121
$10^6 M_{\odot}$	$100r_{\text{g}}$	$1.0 \times 10^4 \text{ km s}^{-1}$	1
$10^6 M_{\odot}$	$100r_{\text{g}}$	$2.0 \times 10^4 \text{ km s}^{-1}$	0.7385
$10^7 M_{\odot}$	$100r_{\text{g}}$	$1.5 \times 10^4 \text{ km s}^{-1}$	0.8873
$10^8 M_{\odot}$	$100r_{\text{g}}$	$1.5 \times 10^4 \text{ km s}^{-1}$	0.8873

explosion ejecta. For each part of the ejecta, the initial position and velocity are taken as the position and velocity of the ejecta at the explosion point, respectively. The trajectory of each part of the ejecta can then be determined, allowing us to determine whether it falls back to the disc, and, if so, obtain its time, position, and velocity. Since the fallback ejecta is typically dispersed widely upon reaching the disc, the mass of the fallback ejecta per  $r_{\text{g}}$  is lower than the mass of the disc gas per  $r_{\text{g}}$  (with exceptions discussed in Section 3). The impact of the fallback ejecta on the fast-rotating disc gas leads to the generation of shock waves, which efficiently convert kinetic energy into internal energy, thereby resulting in the production of electromagnetic radiation. It is assumed that, once the fallback ejecta has swept a mass equal to itself in the disc, all the kinetic energy is converted into internal energy and the dissipated energy for each part of the ejecta can be expressed as

$$E_i = \frac{1}{2} \frac{M_{\text{ej}}}{N} v_{\text{rel}}^2, \quad (4)$$

where  $M_{\text{ej}}$  represents the mass of the explosion ejecta and  $v_{\text{rel}}$  is the relative velocity between the fallback ejecta and the disc gas. It should be noted that different parts of the ejecta generally exhibit different  $v_{\text{rel}}$ . However, only a portion of the energy can be released as electromagnetic radiation, and the efficiency is conservatively set to approximately  $\eta \sim 5\%$ . This value encompasses the uncertainty of the model and ensures the validity of the qualitative analysis. Thus, for each part of the ejecta, only the energy  $\eta E_i$  is converted into electromagnetic radiation. This efficiency is similar to that assumed in the simulations conducted by [Jiang et al. \(2016\)](#), which studied the collisions of debris from a tidal disruption event (TDE). Although the kinetic energy of the debris stream is not completely converted into internal energy in these simulations, the final radiation efficiency is still 2% - 8%. [Wilson & Mathews \(2004\)](#) qualitatively estimated that the radiation energy resulting from a SN Ia explosion impacting an AGN disc is approximately  $10^{50}$  erg. This radiation energy is equivalent to a radiation efficiency of  $\sim 5\%$ .

Setting  $M_{\text{SMBH}} = 10^7 M_{\odot}$ , explosion radius  $R_{\text{ej}} = 100r_{\text{g}}$ , explosion velocity  $v_{\text{ej}} \sim 1.5 \times 10^4 \text{ km s}^{-1}$  and ejecta mass  $M_{\text{ej}} = 1.8M_{\odot}$  as our fiducial model parameters, the corresponding fallback ejecta ratio (ratio of the total mass of fallback ejecta versus the total mass of ejecta) is 0.8873. The effects of varying the model parameters on the fallback ejecta ratios are shown in Table 2. Because the escape velocity decreases with increasing explosion radius, a larger explosion radius or explosion velocity yields a smaller fallback ratio. The SMBH mass does not affect the fallback ratio. For all cases



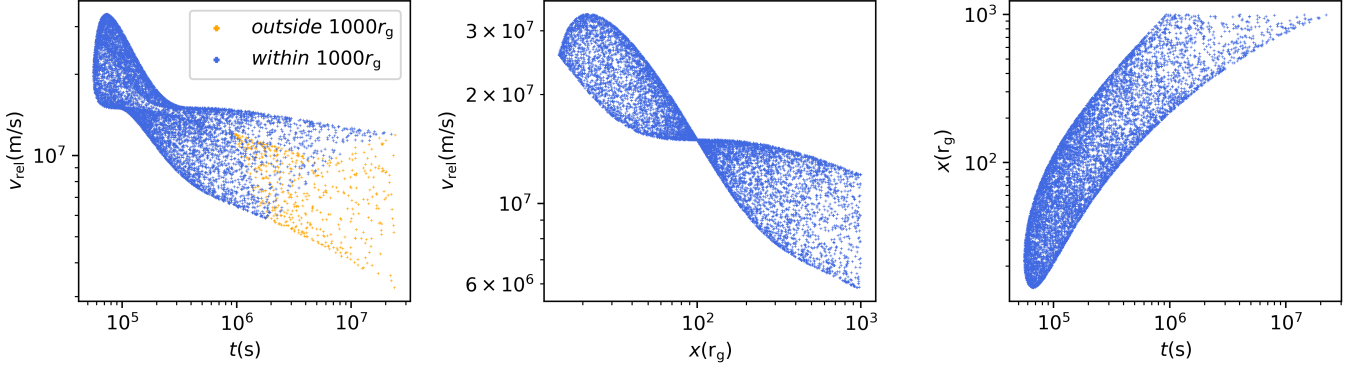


**Figure 2.** Physical properties of the ejecta that fall back onto the AGN disc in the fiducial model. The **left panel** gives the relationship between  $v_{\text{rel}}$  and the fallback time, the blue points represent the ejecta that fall back within  $10^3 r_g$  while the orange points represent the ejecta that fall back outside  $10^3 r_g$ . The **middle panel** shows the relationship between the  $v_{\text{rel}}$  and the fallback position, and the **right panel** illustrates the relationship between the fallback position and the fallback time.

considered here, more than half of the ejecta fall back towards the disc.

### 3 LIGHT CURVE

With a given set of model parameters for a supernova explosion, the fallback ratio, along with the ejecta falling information including the time, position, and velocity, can be obtained. This allows us to calculate the rate of ejecta fallback and the rate of energy dissipation with time, and hence the light curve.

The scatter diagram in Fig. 2 illustrates the physical properties of the fallback ejecta. The left panel shows the relationship between  $v_{\text{rel}}$  and the fallback time; the middle panel gives the relationship between  $v_{\text{rel}}$  and the fallback position; and the right panel shows the relationship between the fallback position and the fallback time. Each point represents one part of the fallback ejecta. In order to improve distinguishability, the scatter plot has been refined by using the results with  $N = 2 \times 10^4$ . In the left panel, the orange points represent the ejecta falling back within  $10^3 r_g$ , while the blue points represent those that fall back outside  $10^3 r_g$ . During the early period, the relative velocity is widely dispersed, and can be up to  $3.5 \times 10^7 \text{ m s}^{-1}$ . Therefore, the average dissipated energy for each ejecta is relatively large at this time. At the later time ( $> 10^6 \text{ s}$ ), the relative velocity is distributed below  $1.5 \times 10^7 \text{ m s}^{-1}$ . As time goes by, the distribution of the relative velocity changes slowly, and the average dissipated energy for the ejecta decreases gradually. Similarly, in the middle panel, the ejecta falling at  $\lesssim 100 r_g$ , the relative velocity is more dispersed, the average relative velocity is larger, and so each part of the ejecta dissipates more energy. At  $\gtrsim 100 r_g$ , the average relative velocity becomes smaller and the energy dissipation for each part of the ejecta is less. Generally speaking, for the farther fallback position the relative velocity is found to be lower. At  $\sim 100 r_g$ , there is a point where the relative velocity is concentrated at  $\sim 1.5 \times 10^7 \text{ m s}^{-1}$ . From the right panel, it can be seen that, during the early period, fallback positions are in the inner region of the disc ( $\sim 15 r_g$ ). Later on, the fallback positions increase rapidly, and the average distance of the fallback positions increases rapidly as well. This is because a longer time of movement is usually required for points falling farther from the SMBH. In general, the fallback ejecta are dispersed in time and space.

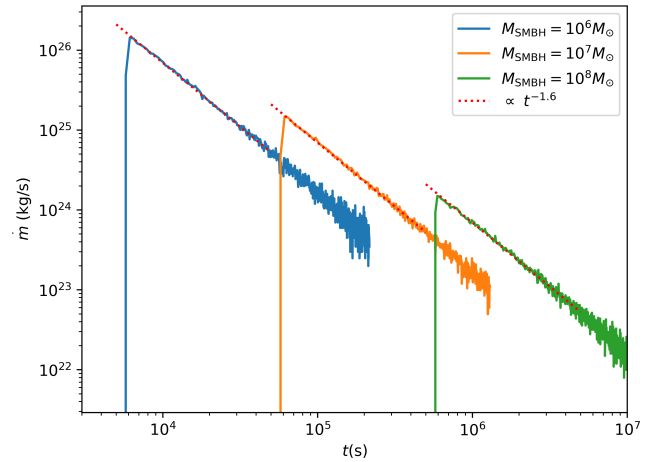


**Figure 3.** The rate of the fallback mass as a function of time. Different solid lines correspond to the cases with the different SMBH masses. The red dotted line follows  $L \propto t^{-1.6}$ . The rest of the parameters are taken from the fiducial model.

In the following, we first examine the effects of the SMBH mass, while keeping the other parameters fixed to those of the fiducial model. At  $100 r_g$ , the Keplerian velocity is  $c/10$ , which is greater than the explosion velocity of a supernova. Therefore, in the fiducial model, all ejecta is still along the side of the moving direction of the center of mass (i.e. the Y-component of all ejecta velocities is positive). It is also worth noting that the relative velocities for collisions with  $c/10$  have a relativistic correction of less than 1%. This indicates that the relativistic effects of ejecta are relatively negligible in this scenario.

Fig. 3 shows the rate of the fallback rate as a function of time. Different lines correspond to the different SMBH masses, which are  $M_{\text{SMBH}} = 10^6 M_{\odot}, 10^7 M_{\odot}$  and  $10^8 M_{\odot}$ , respectively. The profiles of different lines are almost the same, but the fallback time-scale is different due to the different central SMBH masses. Since the total ejecta masses are the same, that is, the amount of the material ejected from a SN Ia explosion, the peak fallback rate decreases by an order of magnitude as the SMBH mass increases by an order of magnitude.

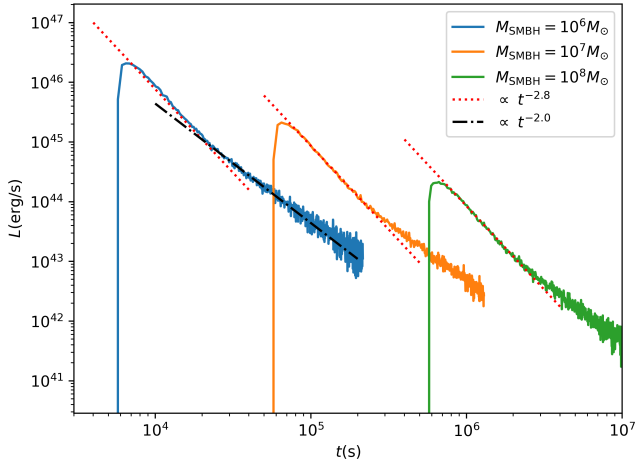


**Figure 4.** The light curves originating from the energy dissipation caused by fallback ejecta hitting the disc gas. The red dotted lines and black dashed line follow  $L \propto t^{-2.8}$  and  $L \propto t^{-2.0}$ , respectively. The rest of the parameters are the same as these of the fiducial model.

The jaggedness in the curves results from the finite number used in the simulations ( $N = 2 \times 10^5$ ), which can be improved by increasing  $N$ .

Fig. 4 shows the light curves. The profiles of the light curves are similar to the time evolution of the rate of the matter fallback, characterized by a fast rise and then followed by a power-law decay. However, the light curve is related not only to the fallback rate but also to the corresponding  $v_{\text{rel}}$  and parameter  $\eta$  in our model. For comparison, the curves  $L \propto t^{-2.8}$  and  $L \propto t^{-2.0}$  are also plotted. In the initial period after the peak in the light curve, the luminosity decreases rapidly with a power law  $L \propto t^{-2.8}$ , and then with a moderate power law  $L \propto t^{-2.0}$  in the subsequent period. The overall decline index is high, meaning the luminosity changes rapidly. Different SMBH masses do not affect the light-curve profile, but they do influence the time-scale of variability and peak luminosity. As SMBH mass increases by an order of magnitude, the time-scale of variability also increases an order of magnitude, and the peak luminosity decreases by an order of magnitude. These trends offer the possibility of using the variability timescale to constrain the mass of the SMBH.

The effects of different parameters from the fiducial model are shown further in Figs 5 – 7. The light curves of different explosion velocities are compared in Fig. 5. It can be seen from Table 2 that the fallback ratio of ejecta decreases with increasing explosion velocity. From the light curves, however, it is found that a larger explosion velocity, resulting in higher  $v_{\text{rel}}$ , can lead to an earlier peak time and a larger peak luminosity, although the power-law shape of the light curve remains unchanged. A lower explosion velocity ( $v_{\text{rel}} = 10^4 \text{ km s}^{-1}$ ) means that the ejecta is affected by the AGN disc and partially is decelerated during the initial phase; or it can mean that the explosion result deviates from the ideal collision with zero impact parameter (Raskin et al. 2009). The light curves for the cases of the different ejecta masses are compared in Fig. 6. Different ejecta masses can only change the peak luminosity while keeping the peak time and the profile of light curves unchanged.

The light curves for the cases of the different explosion radii are compared in Fig. 7. Different explosion radii affect the profile of the light curve. It is worth noting that the green curve corresponding to the explosion radius at  $500r_g$  has two peaks. This is because the

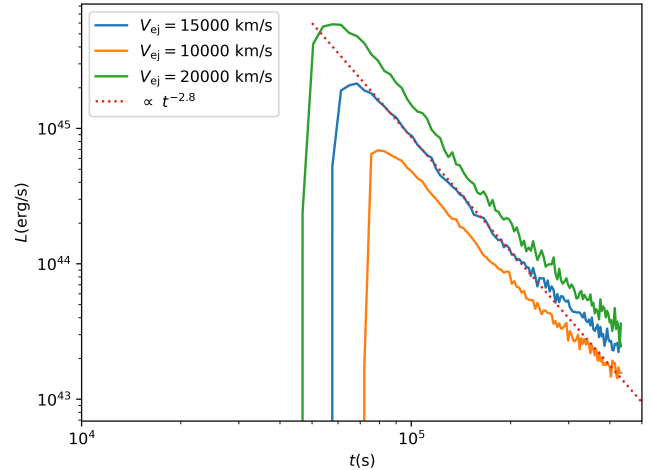


**Figure 5.** Light curves for different explosion velocities, compared with the fiducial model and  $L \propto t^{-2.8}$ .

Kepler velocity at  $500r_g$  is lower than the explosion velocity. In contrast to the explosion at  $100r_g$ , the ejecta after the explosion still moves along the direction of the side of the center of mass, but some parts of the ejecta along the opposite side in  $500r_g$  case (i.e. the Y-component of some ejecta velocities is negative.) These parts of the ejecta produce two peaks in the light curve. For the larger explosion radii or larger explosion velocity, the fallback ratio is smaller (Table 2). However, it is obvious that the peak value of the light curve is not determined by the fallback ratio alone. Generally, two physical factors affect the power-law slopes of the light curve: the fallback rate of ejecta and the change rate of the average relative velocity between the fallback ejecta and the disc gas. In the case of a single light curve, while the fallback rate of ejecta varies with time following a power-law slope (as shown in Fig. 3), the relative velocity does not vary with time following a power-law slope (as shown in Fig. 2). Therefore, the change in the average relative velocity over time is the factor responsible for the different power-law slopes of the same light curve at different times. When comparing different light curves, their fallback rate of matter and the change rate of average relative velocity differ, resulting in varying curve profiles and power-law slopes.

Several assumptions are made in the above calculations. When the ejecta falls back onto the AGN disc, it interacts primarily with the surface material of the disc. Radiation can escape the disc promptly, since the optical depth in this location is not too large (see Section 4 for estimates). It is assumed that the fallback ejecta is completely absorbed by the disc gas and that the kinetic energy is converted into internal energy, with efficiency  $\eta \sim 5\%$  converting internal energy into electromagnetic radiation. However, as shown in Fig. 8, this assumption does not hold in the inner part of the AGN disc: for  $M_{\text{SMBH}} = 10^6 M_\odot$ , the falling ejecta stream is heavy enough to penetrate the disc. The term ‘heavy’ means that the time-integrated fallback ejecta per unit radius is greater than the disc gas per unit radius; this should not be confused with ‘heavy element’. In Fig. 8, the blue curve represents the time-integrated distribution of the fallback ejecta in the AGN disc, which is compared with the different distributions of AGN disc gas. The blue curve is taken from the fiducial parameters, but it is suitable for the different central SMBH masses. The heavy falling stream can affect the stable structure of the AGN disc. We do not quantitatively consider the destruction of the disc and subsequent effects further, but such processes should

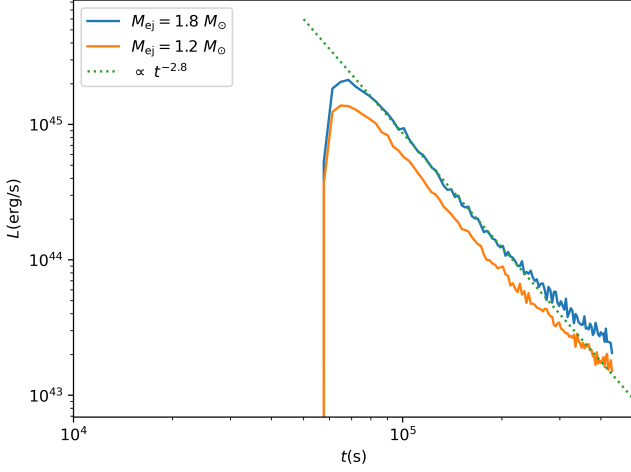


**Figure 6.** Light curve for different ejecta mass, compared with the fiducial model and  $L \propto t^{-2.8}$ .

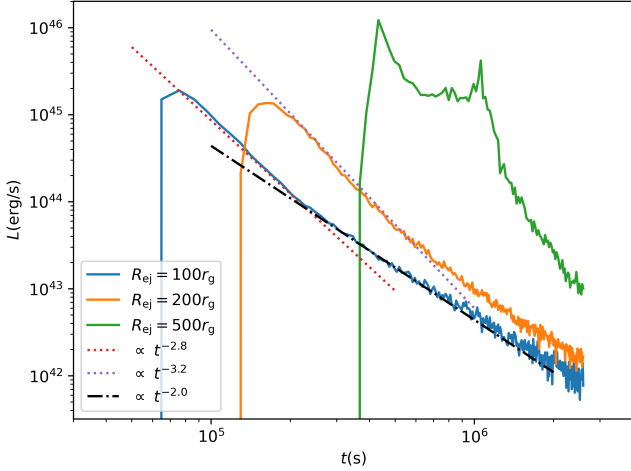


**Figure 7.** Light curves for different explosion positions, compared with the fiducial model and  $L \propto t^{-2.8}$ .

be correlated with changing-look AGN, as described in the model for the source 1ES 1927+654 [Trakhtenbrot et al. \(2019\)](#); [Ricci et al. \(2020\)](#); [Li et al. \(2022a\)](#). Therefore, the peak range of the actual light curve should deviate from the blue curve of Fig. 3. However, it is still reliable and can approximate the light curve at this time. Because the fallback ejecta is symmetrical about the AGN disc plane, the velocity in the  $Z$ -direction can cancel out, and only a small part of the kinetic energy is consumed by the AGN disc.

#### 4 SPECTRAL ENERGY DISTRIBUTION

Suppose that after collisions between the fallback ejecta and AGN disc gas with equal masses, all kinetic energy is converted into thermal energy through shocks. Radiation of the thermal energy can be approximated with a blackbody spectrum. The optical depth at the shock location can be estimated as,

$$\tau \sim \sigma \frac{\Sigma}{2m_{\text{H}}}, \quad (5)$$

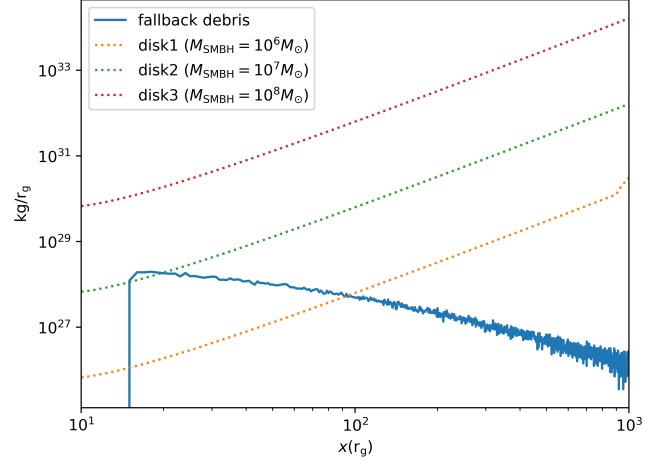


**Figure 8.** The time-integrated distribution of the fallback ejecta in AGN disc (blue curve) compared with the different distribution of AGN disc gas (orange, green and red dotted curves represent  $M_{\text{SMBH}} = 10^6 M_{\odot}$ ,  $10^7 M_{\odot}$ ,  $10^8 M_{\odot}$  respectively). The blue curve show the result of the case with the same fiducial parameters but the different masses of the central SMBH.

here,  $\sigma$  represents the cross section of photons, and  $\Sigma$  denotes the average column density of the fallback ejecta, which can be estimated from Fig. 8. The cross-section for radiation can be written as ([Rybicki & Lightman 1991](#)),

$$\sigma = \frac{3}{4} \sigma_{\text{T}} \left\{ \frac{1 + \Gamma}{\Gamma^3} \left[ \frac{2\Gamma(1 + \Gamma)}{1 + 2\Gamma} - \ln(1 + 2\Gamma) \right] + \frac{\ln(1 + 2\Gamma)}{2\Gamma} - \frac{1 + 3\Gamma}{(1 + 2\Gamma)^2} \right\}, \quad (6)$$

where  $\sigma_{\text{T}}$  is the Thomson cross section and  $\Gamma$  is the ratio of photon energy to the rest energy of electron, which is defined as

$$\Gamma = \frac{h\nu}{m_e c^2}, \quad (7)$$

where  $h$  is the Planck constant,  $m_e$  is the rest mass of electron, and  $\nu$  is the photon frequency. In our fiducial model, the fallback location is at  $\sim 100 r_{\text{g}}$  ( $\Gamma \sim 10$ ), the thickness is  $\tau \sim 80 \gtrsim 1$ , and thus the blackbody spectrum approximation is reasonable. The total SED during a period of time is determined by the superposition of all blackbody spectra.

Assuming that the average molecular weight of ejecta is  $m_A = Am_{\text{H}}$ , and considering that the AGN disc comprises ionized hydrogen, the temperature  $T$  can be calculated using the equipartition theorem,

$$\frac{1}{2} m_A v_{\text{rel}}^2 = \frac{3}{2} \left( 1 + A + \frac{3}{2} A \right) k_{\text{B}} T. \quad (8)$$

It follows that

$$T = \frac{2Am_{\text{H}}v_{\text{rel}}^2}{3(2 + 5A)k_{\text{B}}}, \quad (9)$$

where  $k_{\text{B}}$  is Boltzmann constant. When  $A \gg 1$ ,

$$T \simeq \frac{2m_{\text{H}}v_{\text{rel}}^2}{15k_{\text{B}}}. \quad (10)$$

For  $M_{\text{SMBH}} = 10^6 M_{\odot}$ , if the fallback ejecta is located in the inner region of the AGN disc ( $< 100 r_{\text{g}}$ ), it is assumed that the fallback

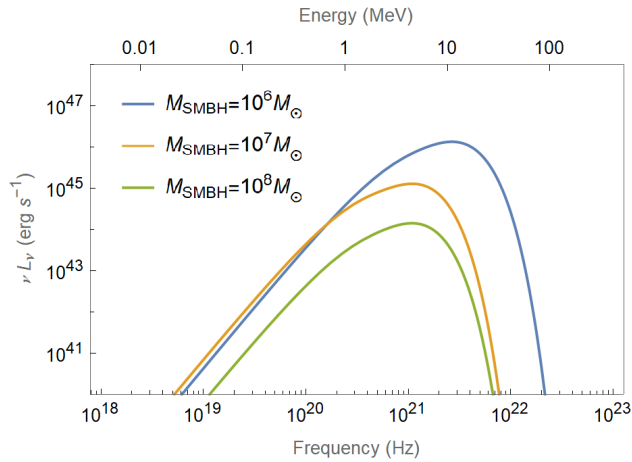


**Figure 9.** The SEDs at the peak luminosity for different SMBH masses. The rest of the parameters are taken from the fiducial model. The multi-temperature black body spectra are created by overlaying the SEDs generated by each part of the fallback ejecta.

ejecta mainly collides with the symmetrical part of the fallback ejecta, resulting in

$$\frac{1}{2}m_A v_{\text{rel}}^2 = \frac{3}{2}(2+A)k_B T, \quad (11)$$

and the temperature is

$$T = \frac{Am_H v_{\text{rel}}^2}{3(2+A)k_B}. \quad (12)$$

When  $A \gg 1$ ,

$$T \approx \frac{m_H v_{\text{rel}}^2}{3k_B}. \quad (13)$$

Fig. 9 illustrates the SED at the peak luminosity for the cases of the different SMBH masses. It can be observed that the peak luminosity increases as the SMBH mass decreases, which is consistent with the results presented in Fig. 4. All these SEDs exhibit multi-temperature blackbody spectra, with peak frequencies falling within the soft  $\gamma$  range. Notably, for  $M_{\text{SMBH}} = 10^6 M_\odot$ , the SED peaks at a relatively higher frequency. This is because in the case of a less massive central SMBH, the disc gas in the inner region is not sufficiently dense and thus the fallback ejecta dissipates energy primarily through collisions with the symmetrical part of the ejecta. As a result, radiation of relatively higher energy is produced. For SMBHs of other masses ( $M_{\text{SMBH}} \gtrsim 10^7 M_\odot$ ), the energy is dissipated by collisions between the fallback ejecta and the disc gas. This difference can be seen by comparing Equations (9) and (12). According to the equipartition theorem, the average energy of each particle obtained from kinetic energy dissipation is different, because the composition of the fallback ejecta is different from that of the AGN disc gas. However, the definition of  $v_{\text{rel}}$  in Equations (8) and (11) is the same (the relative velocity between the fallback ejecta and the disc gas). Since the fallback ejecta exhibits symmetry with respect to the AGN disc, the Z-component of the velocity cancels out and only a small portion of the remaining kinetic energy is transferred to the AGN disc.

Figs 10 and 11 show the SEDs for the cases of  $M_{\text{SMBH}} = 10^6 M_\odot$  and  $M_{\text{SMBH}} = 10^7 M_\odot$ , respectively. The lines in the different colors represent the SED at the different times. At the maximum of the light curve, the peak frequency of the SED is in the soft  $\gamma$  range due

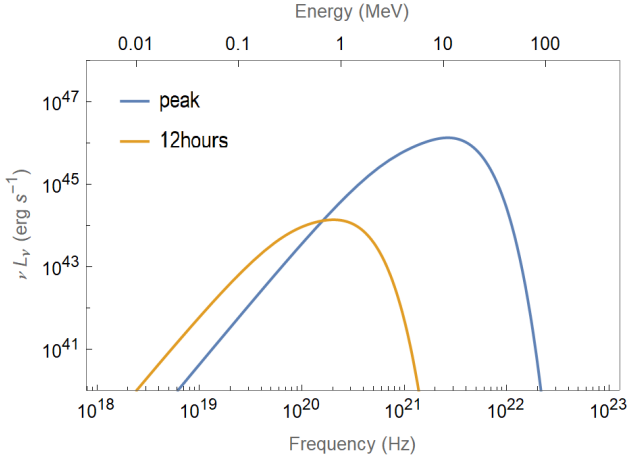
to the large  $v_{\text{rel}}$ , but at late times the peak frequency shifts into the hard X-ray range. Except for some blazars, the average luminosities of AGNs at MeV energies are  $\lesssim 10^{40} \text{ erg s}^{-1}$  (Hubeny et al. 2001). Therefore, the high-energy radiation caused by the fallback ejecta of SNe Ia when it hits the disc gas far exceeds the AGN background luminosity and it should be detectable.

Fig. 12 shows the light curves in different energies around the MeV range for the fiducial model. The red dotted line indicates the peak time of the total luminosity, and the light curves in different energies are shown from the peak time. It can be seen from the figure that the higher the energy, the faster the curve varies. Although the peak luminosity of 10MeV is very high, reaching about  $\gtrsim 10^{40} \text{ erg s}^{-1}$ , it rapidly decreases by about 10 orders of magnitude within 6 days from the peak time; the luminosity of 1MeV only decreases by about one order of magnitude within 6 days; while the luminosity of 0.1MeV keeps almost as a constant within 6 days. Therefore, the high energy radiation of  $\gtrsim 10\text{MeV}$  is mainly concentrated near the peak time of the total luminosity, while the low-energy radiation can last for a relatively long time. These trends are the same for the SMBHs with the different masses, but the time-scales vary with the mass of the SMBH, correspondingly. We also notice that the luminosity in the 0.1MeV band increases (rather than decreases) after the peak of the total luminosity for  $M_{\text{SMBH}} = 10^6 M_\odot$ . This feature can also be seen in Fig. 10, and is caused by the collisions between symmetrical fallback ejecta in the inner part of the AGN disc. In contrast, the light variation resulting from the initial explosion and radioactive decay of SNe Ia is not influenced by the mass of the SMBH. This is due to the fact that the half-life of radioactive elements involved in the decay process remains constant.

For comparison, Wilson & Mathews (2004) estimated a peak photon energy of approximately 400keV for SNe Ia ejecta impacting an AGN disc. Additionally, Chan et al. (2021) calculated that the fallback debris from a TDE colliding with an AGN disc generates a photon energy peak of up to  $\sim \text{MeV}$ . A more comprehensive discussion on the limitations of the estimated SEDs has been provided in Section 5.1.

The sky at MeV energies is currently poorly explored. From Fig. 12, it is evident that the luminosity in the fiducial model at an energy of 1MeV is approximately  $10^{43} \text{ erg s}^{-1}$ . According to our estimation, *Fermi* Gamma-ray Burst Monitor (GBM: Meegan et al. 2009) could detect the gamma-ray emission at 1MeV resulting from the collision of binary WDs in AGNs within only 1 Mpc. However, some of our predicted events, with peak energies estimated to be around 10-50 MeV, might be detectable in *Fermi* data using the Large Area Telescope (LAT) Low-Energy technique, which can significantly increase the effective area down to 30 MeV (Pelassa et al. 2010). Our predicted event may also be observed by future MeV detectors such as Compton Spectrometer and Imager (COSI) (Tomsick & COSI Collaboration 2022), Cube Sat MeV telescope (MeVCube) (Lucchetta et al. 2022), e-ASTROGAM (de Angelis et al. 2018), ComPare (Shy et al. 2022; Moiseev et al. 2015), the All-sky Medium Energy Gamma-Ray Observatory eXplorer (AMEGO-X) (Fleischhack 2021), the Galactic Explorer with a Coded aperture mask Compton telescope (GECCO) (Orlando et al. 2022), and the Advanced Particle-Astrophysics Telescope (APT) (Buckley & APT Team 2022). Taking AMEGO-X as an example, its sensitivity at the 1MeV energy is  $5 \times 10^{-6} \text{ MeV cm}^{-2} \text{ s}^{-1}$  (Fleischhack 2021), so AMEGO-X can detect our predicted burst at  $\sim 100\text{Mpc}$ . This distance is much larger than the known nearest Seyfert galaxy (Filippenko & Ho 2003).





**Figure 10.** The SEDs at different times for  $M_{\text{SMBH}} = 10^6 M_{\odot}$ . The blue curve corresponds to the phase when the light curve is at its peak, and the orange curve corresponds to 12 hours after the explosion. The rest of the parameters are taken from the fiducial model.

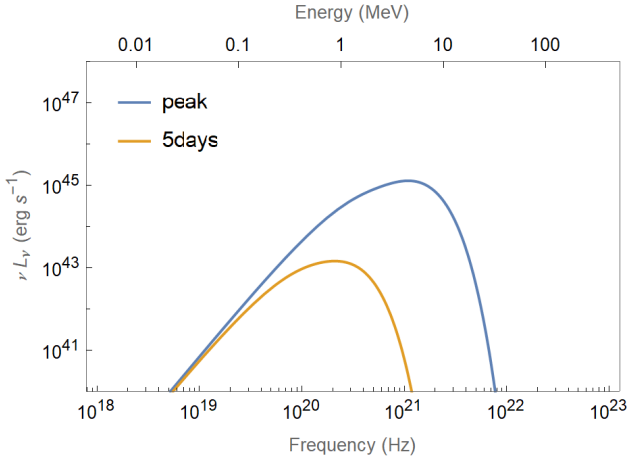


**Figure 11.** The SEDs at different times for the fiducial model. The blue curve corresponds to the phase when the light curve is at its peak, and the orange curve corresponds to 5 days after the explosion.

## 5 DISCUSSION

### 5.1 Model uncertainties

Because a significant WD population within the disc is a key facet of our model, it is necessary to discuss this assumption in greater detail. The initial mass of stars in the AGN disc environment can be ‘top heavy’ due to the high gas density in the disc, and the accretion of stars can change the distribution of the stellar mass further. However, it can be seen from fig. 7 of [Derdzinski & Mayer \(2022\)](#) that the peak value of stellar initial mass functions (IMFs) is under  $8M_{\odot}$  except for  $M_{\text{SMBH}} = 10^6 M_{\odot}$ , and a star below  $8M_{\odot}$  can evolve into a WD. Even after  $10^6$  years of accretion, the peak value of the stellar mass function in an AGN disc with  $M_{\text{SMBH}} = 10^6 M_{\odot}$  can still reach below  $8M_{\odot}$ . Moreover, the stellar mass function is also related to the location in an AGN disc: for instance, the characteristic mass of protostar formed by in situ collapse is smaller in the inner region of the AGN disc (e.g. fig. 5 of [Derdzinski & Mayer \(2022\)](#)).

It is noteworthy that the AGN disc lifetimes may be less than the

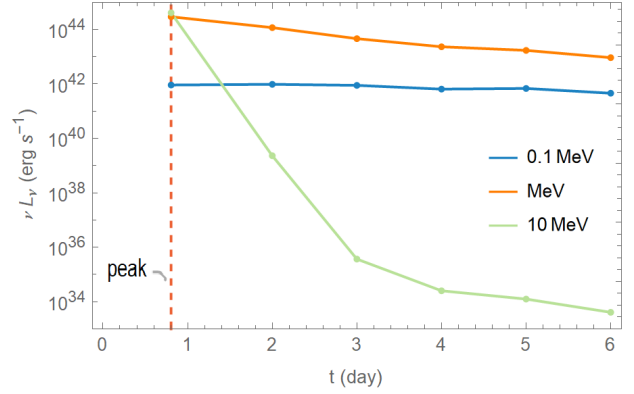


**Figure 12.** The light curves in different energies around the MeV range for the fiducial model. The red dotted line indicates the peak time of the total luminosity, and the light curves in different energies are showed from the peak time.

main-sequence lifetimes of low-mass stars. According to the duty cycle model of AGNs (e.g. [Shankar et al. 2009](#)), although stars cannot evolve to WDs in one AGN activity cycle, they may evolve to WDs in the subsequent activity cycles or during periods of quiescence in the nucleus.

Additionally, mass segregation in nuclear star clusters should cause WDs to occupy areas further from the centre compared with BHs or neutron stars (NSs), but not all nuclear clusters exhibit effective mass segregation ([McKernan et al. 2020](#)). Around more massive SMBHs ( $\gtrsim 10^7 M_{\odot}$ ), mass segregation may be less efficient and a less top-heavy IMF may be more appropriate. Such a circumstance should also apply to stars or compact objects that are captured into the disc.

For the capture of stars, their characteristic stellar mass can be lower than that of in situ collapse. While the accretion of captured stars in the inner region of an AGN disc increases the mass that could result in the formation of BHs, this is not the case in the outer region of the AGN disc ([Cantiello et al. 2021](#)). Following the accretion and evolution of stars, WDs formed in the outer region of the AGN disc can migrate to the inner region without undergoing collapse into BHs. In general, the IMF of stars in AGN discs tends to be ‘top heavy,’ with further mass increase through accretion. However, the initial mass, accretion, and evolution of stars are also influenced by their positions in the discs and the properties of the discs. Considering all these conditions, a significant number of WDs can still be generated in AGN discs.

Another facet of caution is the presence of migration traps. Although many works predict that migration traps exist in locations we are currently investigating, [Dittmann & Miller \(2020\)](#) did not find any migration traps in their disc models. [Pan & Yang \(2021a\)](#) also suggested that including headwinds in migration leads to the complete disappearance of migration traps. Actually, our results do not necessarily rely entirely on migration traps, but we still expect the new observable phenomenon proposed in our paper to occur mainly at locations within  $\lesssim 10^3 r_g$ . The reasons are as follows. (i) Apart from migration traps, an overdensity of disc compact objects can also occur in regions of varying aspect ratios or varying migration time-scales ([McKernan et al. 2014](#)). According to [McKernan et al. \(2012\)](#), the migration time-scale of  $1 - M_{\odot}$  compact stars increases inwards at  $\lesssim 10^3 r_g$ , although only the Type I migration torque is included. Alternatively, as depicted in fig. 3 of [Peng & Chen \(2021\)](#),

the effects of GW torque and gas torque are considered. When the radius of the AGN disc decreases, the torque decreases or the migration timescale increases in the relative outer region of the AGN disc ( $\sim 10^3 r_g$ , which is not the trap region). Therefore, collisions may have occurred before WDs are migrated to traps due to the differential migration time-scale. (ii) Our simulations show that even if there are two WDs close to each other (the orbital separation of the two WDs is less than  $2\sqrt{3}R_H$ ), the probability of collision in the outer part of AGN disc can be reduced (Luo et al. 2023). (iii) Even if a small number of WDs collide in the outer region of AGN discs, the observational effect may not be obvious due to large amounts of the gas, unless the shock wave can break out on the disc surface (Zhu et al. 2021b). Even though the very external regions ( $\gtrsim 10^4 r_g$ ) of a disc may initially be neutral, the early radiation from the explosion itself can ionize the neutral gas at a very short time-scale (Perna et al. 2021). The ionization leads the disc to become optically thick, and the ejecta also can not rush out of the disc. In such cases, there might not be an overtly observable effect, but there is feedback on AGN discs. However, as noted by Gilbaum & Stone (2022), the feedback is relatively insignificant compared to the accretion of compact objects. Alternatively, as in Grishin et al. (2021), the ejecta can rush out of the disc if they are not in the midplane of the disc, but the explosion velocity is greater than the escape velocity, resulting in a significant portion of the ejecta escaping from the disc. The ejecta may also be partially decelerated before it rushes out of the disc so that the ejecta can fall back. If so, the explosion height needs to be precisely adjusted, which seems very unphysical.

For lower mass SMBHs, the light curve and SED at peak luminosity need to be corrected. As shown in Fig. 8, the fallback ejecta at the inner radius of a SMBH with  $M_{\text{SMBH}} \sim 10^6 M_\odot$  is sufficiently massive that it can induce changes in the structure of the AGN disc. Considering that not all the kinetic energy of the fallback ejecta is converted into thermal energy, some part of the fallback ejecta may deviate from a blackbody spectrum. However, it is still a reliable approximation to estimate the SED at this time due to the symmetrical nature of the fallback ejecta around the AGN disc. As a result, the Z-component of the velocity cancels out, and only a small fraction of the kinetic energy is consumed by the AGN disc.

In Section 4, we demonstrate that blackbody emission necessitates an optically thick medium but also requires efficient emission processes. The caveat of this key assumption should be discussed in more details. If the ejecta falls back at a relatively small distance ( $\lesssim 10^3 r_g$ ), free-free cooling dominates, but insufficient high-energy photons from free-free radiation can cause the spectrum to deviate from the blackbody spectrum. This results in a Wien spectrum at high frequencies dominated by inverse Compton and a flat spectrum at low frequencies dominated by free-free emission (Nakar & Sari 2010; Linial & Metzger 2023). Nonetheless, it is expected that this deviation to not be significant because there are enough low-energy photons (Katz et al. 2010) to couple with hot electrons, and soft photons from the AGN disc can serve as seed photons for the inverse Compton scattering. If the fallback position is farther away ( $\gtrsim 10^3 r_g$ ), the fallback ejecta become highly dispersed and optically thin, resulting in the domination of inverse Compton radiation, with the seed of soft photons originating mainly from the AGN disc. However, the actual radiation spectrum is complex, and the above-mentioned radiation mechanisms can coexist and evolve with time. Various corrections, such as the generation of positron-electron pairs and possible magnetic effects, should also be considered. Although the temperature calculated from Equations (9) and (12) can reach up to  $\sim 10^{11}$  K, we have ignored the pair production. Therefore, the multi-temperature blackbody used in this paper as a preliminary ap-

proximation to the complex radiation process has some limitations, and further study of the detailed radiation processes and radiation transfer is necessary to obtain the more realistic spectrum.

## 5.2 Potential implications

In this study, the calculation of trajectories and the disc model does not incorporate general relativity (GR). It is assumed that collisions occur at distances  $\lesssim 10^3 r_g$ ; these collisions may have already taken place before the WDs reach the innermost region. For example, at  $\sim 100 r_g$ , GR effects (the change of fallback time of debris and the change of relative velocity due to the precession) are far less than other effects such as SMBH mass and explosion velocity. Therefore, as a leading-order result, it is reasonable for us to calculate trajectories in Newtonian mechanics. However, GR calculation is indispensable if some collisions occur in the very inner region ( $\sim 10 r_g$ ). Such reasoning should also apply to the AGN disc model; the effect of GR on the disc model is also the sub-leading effect outside the very inner region. In addition, as long as the accretion rate is not too high, the difference between the actual angular velocity of the disc gas and the Keplerian angular velocity is very small (Peng & Chen 2021), so the model of Kato et al. (2008) is sufficient for our discussions.

If not all WDs collide outside the very inner region, some WDs can continue on their paths until they collide in the last migration trap (Peng & Chen 2021) or fall into the SMBH. When WDs collide in the very inner region, additional GR effects are expected. One such effect is related to the optical radiation of SN Ia, which mainly originates from radioactive decay. The decay time is measured in the local proper time and, as a result of GR, the decay time seen by distant observers might appear longer compared to that of a normal SN Ia. It should be noted that observing this effect is challenging, since one needs to wait for a certain amount of time after the peak luminosity to measure it, during which the luminosity is already lower than the AGN background.

Furthermore, there are other potential effects to consider. First, an extreme mass ratio inspiral (EMRI) occurs before the collision of the WDs, accompanied by the corresponding GW signal. If the WDs collide in the very inner region, the GW signal abruptly disappears after the collision. Second, the initial explosion can cause significant destruction to the AGN disc, resulting in a substantial decrease in AGN luminosity, while the SN Ia luminosity, particularly in the optical band, increases significantly. Third, in the very inner region of the AGN disc, where the explosion velocity is much lower than the escape velocity, the accretion of fallback ejecta can form an accretion disc. This transient source exhibits similarities to a TDE. Quantitative calculations of these effects would require the application of general relativistic magnetohydrodynamics, coupled with radiation transfer simulations. However, such detailed techniques extend beyond the scope of this paper and will be addressed in future work.

The destruction of the AGN disc can result in an elevated accretion rate and fluctuations in AGN luminosity, potentially leading to the manifestation of a changing-look AGN. The radiation from the initial explosion and its impact on the AGN disc should be considered. The explosion is similar to normal SN Ia, but the AGN's radiation and the subsequent effects should also be taken into account. Based on the result from Contardo et al. (2000), the initial explosion luminosity of SNe Ia can reach  $\sim 10^{43}$  erg s $^{-1}$ . In the example provided by Zhu et al. (2021a), when the AGN accretion rate is 0.3 times the Eddington accretion rate and the SMBH mass is  $\lesssim 10^7 M_\odot$ , the AGN optical luminosity is  $\lesssim 10^{43}$  erg s $^{-1}$ . Therefore, within a reasonable range of parameters, the optical luminosity of AGN can be lower than that of a SN Ia explosion, although some may be comparable.

The motion of the radioactively decaying ejecta is dominated by the SMBH gravity, which changes the optical depth relative to the observer (MacLeod et al. 2016). The interaction between the disc gas and the supernova ejecta soon after the explosion may lead to a fast early peak in the light curve (Piro & Morozova 2016; Jiang et al. 2021). Another concern is whether the initial explosion can damage the AGN disc significantly. How large is the cavity created by the initial explosion? For our fiducial model in which the initial ejecta sweeps from the AGN disc a mass comparable to its own, we estimate that the radius of the cavity is only  $\sim 5r_g$ . Under these circumstances, the AGN disc experiences only slight damage at the position of the event ( $\gtrsim 100r_g$ ). However, for less massive black holes or thinner discs, the initial explosion may have a significant impact on the disc, and these considerations deserve further investigation.

Our model has broader implications for other explosive events occurring in AGN discs. The kinetic energy of the explosive ejecta in an AGN disc plays a critical role, especially in the inner regions. These explosive events may involve collisions between WDs and BHs or NSs, resulting in micro-TDEs (Perets et al. 2016; Yang et al. 2021). Furthermore, AGN discs can also host other types of collisions, such as NS-NS and NS-BH collisions, or the formation of binaries with very high eccentricities. These events can lead to the ejection of larger amounts of material compared with typical kilonovae (Radice et al. 2016; East et al. 2012; Foucart et al. 2014; Kyutoku et al. 2015), and produce unique GW signatures (Papenfort et al. 2018; Vick & Lai 2019; Wang & Lai 2020). Additionally, AGN discs could potentially serve as sites for the production of heavy elements. For instance, the fallback of SN Ia ejecta onto AGN discs significantly enhances the disc's metallicity and may even contribute to the synthesis of heavy elements within the disc.

## 6 CONCLUSIONS

In the inner region of an AGN disc, the collision between two WDs can lead to a SN Ia explosion through Jacobi capture. This collision is distinct from typical SN Ia events due to the combined effects of the disc gas and the gravitational influence of the SMBH. During the collision, the explosion energy is primarily stored in the ejecta as kinetic energy. Unlike in normal SN Ia events, the AGN disc gas does not decelerate the kinetic energy of the ejecta effectively. Instead, the ejecta rapidly escapes the disc, influenced by the strong gravitational pull of the SMBH. However, a significant portion of the ejecta experiences fallback, returning to the disc. This fallback ejecta is dispersed both in time and spatial position within the disc.

The subsequent interaction between the fallback ejecta and the fast-rotating disc leads to the conversion of kinetic energy into high-energy thermal radiation. This radiation is predominantly emitted in the hard X-ray to soft gamma-ray range.

- In the fiducial model with parameters  $M_{\text{SMBH}} = 10^7 M_\odot$ ,  $R_{\text{ej}} = 100r_g$ ,  $v_{\text{ej}} \sim 1.5 \times 10^4 \text{ km s}^{-1}$ , the peak luminosity resulting from the fallback ejecta impacting the disc can reach approximately  $\sim 10^{45} \text{ erg s}^{-1}$ . Following the peak, the light curve exhibits a rapid decline with a power-law dependence of  $L \propto t^{-2.8}$ , followed by a relatively gentler decay with  $L \propto t^{-2.0}$ . The highest rate of ejecta mass falling back to the AGN disc occurs at a distance of approximately  $\sim 20r_g$ , and the corresponding fallback time for these ejecta is relatively short, aligning with the peak of the light curve. These events may be related to AGN variations on timescales of hours to weeks.

- The variability time-scale in the light curve depends on the mass of SMBH. Specifically, the time-scale increases by approximately an

order of magnitude when the SMBH mass increases by an order of magnitude. However, the overall power-law shape of the light curve remains unchanged. This suggests that the underlying mechanisms governing the variability are determined primarily by the dynamics of the WD collisions and their interaction with the AGN disc, rather than the specific SMBH mass. In the case of an AGN disc with  $M_{\text{SMBH}} \lesssim 10^7 M_\odot$ , the fallback ejecta at the inner radius of the disc can be sufficiently massive to destroy the disc, resulting in a changing-look AGN. The explosion velocity also plays a role in shaping the light curve. A larger explosion velocity leads to a smaller fallback ratio of the ejecta and an earlier time of peak luminosity. However, the overall shape of the light curve remains unchanged. The higher peak luminosity is attributed to the larger explosion velocity, which results in a larger relative velocity between the fallback ejecta and the disc gas. The explosion radius also impacts the light-curve profile. A larger explosion radius leads to a smaller fallback ratio, indicating a reduced mass of ejecta falling back onto the AGN disc. This results in variations in the shape of the light curve. On the other hand, different ejecta masses mainly influence the peak luminosity of the light curve, with no significant impact on the profile of the light curve or the time it takes to reach its peak. The overall shape of the light curve remains consistent, while higher ejecta masses contribute to higher peak luminosities.

- The SEDs of these explosive events, characterized by multi-temperature blackbody spectra that peak in the hard X-ray to soft  $\gamma$  range, could be potentially observed by the future MeV detectors. During the maximum light phase, the peak frequency of the SED is higher compared to later times. This is attributed to the larger relative velocity between the fallback ejecta and the gas within the AGN disc. Specifically, for AGN discs with  $M_{\text{SMBH}} = 10^6 M_\odot$ , the higher peak frequency of the SED arises from collisions between symmetrical fallback ejecta. These collisions contribute to the generation of higher energy photons, resulting in a shift towards higher frequencies in the SED.

Our model has potential implications for other explosive events in AGN discs. By combining future multi-messenger observations (e.g., gravitational waves, neutrinos), we could obtain a more detailed and comprehensive picture of the dynamics and properties of these events, which will provide valuable insights into important topics including AGN variability, the nature of changing-look AGNs, and the origin of heavy elements within AGN environments.

## ACKNOWLEDGEMENTS

We thank the referee for critical suggestions and comments, which are very helpful for the improvement of this work. YFY was supported by the National SKA Program of China No. 2020SKA0120300, and the National Natural Science Foundation of China (Grant No. 11725312). LCH was supported by the National Science Foundation of China (11721303, 11991052, 12011540375, 12233001) and the China Manned Space Project (CMS-CSST-2021-A04, CMS-CSST-2021-A06). JMW acknowledges support from the National Key R&D Program of China (2020YFC2201400, 2021YFA1600404), NSFC (NSFC-11991050, -11991054, -11833008).

## DATA AVAILABILITY

The data underlying this article will be shared on reasonable request to the corresponding author (YFY).

## REFERENCES

- Bartos I., Kocsis B., Haiman Z., Márka S., 2017, *ApJ*, **835**, 165
- Bellovary J. M., Mac Low M.-M., McKernan B., Ford K. E. S., 2016, *ApJ*, **819**, L17
- Boekholt T. C. N., Rowan C., Kocsis B., 2023, *MNRAS*, **518**, 5653
- Buckley J., APT Team 2022, in AAS/High Energy Astrophysics Division. p. 404.04
- Cantiello M., Jermyn A. S., Lin D. N. C., 2021, *ApJ*, **910**, 94
- Chan C.-H., Piran T., Krolik J. H., 2021, *ApJ*, **914**, 107
- Cheng K. S., Wang J.-M., 1999, *ApJ*, **521**, 502
- Contardo G., Leibundgut B., Vacca W. D., 2000, *A&A*, **359**, 876
- Derdzinski A., Mayer L., 2022, arXiv e-prints, p. arXiv:2205.10382
- Dittmann A. J., Miller M. C., 2020, *MNRAS*, **493**, 3732
- Du P., Wang J.-M., Hu C., Valls-Gabaud D., Baldwin J. A., Ge J.-Q., Xue S.-J., 2014, *MNRAS*, **438**, 2828
- East W. E., Pretorius F., Stephens B. C., 2012, *Phys. Rev. D*, **85**, 124009
- Fabj G., Nasim S. S., Caban F., Ford K. E. S., McKernan B., Bellovary J. M., 2020, *MNRAS*, **499**, 2608
- Filippenko A. V., Ho L. C., 2003, *ApJ*, **588**, L13
- Fleischhack H., 2021, *PoS, ICRC2021*, 649
- Foucart F., et al., 2014, *Phys. Rev. D*, **90**, 024026
- Gayathri V., Bartos I., Haiman Z., Klimentenko S., Kocsis B., Márka S., Yang Y., 2020, *ApJ*, **890**, L20
- Gilbaum S., Stone N. C., 2022, *ApJ*, **928**, 191
- Gladman B., 1993, *Icarus*, **106**, 247
- Gopal-Krishna Britzen S., Wiita P., 2019, Bulletin de la Societe Royale des Sciences de Liege, **88**, 132
- Grishin E., Bobrick A., Hirai R., Mandel I., Perets H. B., 2021, *MNRAS*, **507**, 156
- Hawley W. P., Athanassiadou T., Timmes F. X., 2012, *The Astrophysical Journal*, **759**, 39
- Hayden B. T., et al., 2010, *The Astrophysical Journal*, **712**, 350
- Hillebrandt W., Kromer M., Röpke F. K., Ruiter A. J., 2013, *Frontiers of Physics*, **8**, 116
- Hoyle F., Fowler W. A., 1960, *ApJ*, **132**, 565
- Hubeny I., Blaes O., Krolik J. H., Agol E., 2001, *ApJ*, **559**, 680
- Iwamoto K., Kunugise T., 2006, in Kubono S., Aoki W., Kajino T., Motoyayashi T., Nomoto K., eds, American Institute of Physics Conference Series Vol. 847, Origin of Matter and Evolution of Galaxies. pp 406–408, doi:10.1063/1.2234440
- Jiang Y.-F., Guillochon J., Loeb A., 2016, *ApJ*, **830**, 125
- Jiang J.-a., et al., 2021, *ApJ*, **923**, L8
- Kaaz N., Schröder S. L., Andrews J. J., Antoni A., Ramirez-Ruiz E., 2021, arXiv e-prints, p. arXiv:2103.12088
- Kato S., Fukue J., Mineshige S., Disks B.-H. A., 2008, Black-hole accretion disks
- Katz B., Budnik R., Waxman E., 2010, *ApJ*, **716**, 781
- Kroupa P., 2001, *MNRAS*, **322**, 231
- Kyutoku K., Ioka K., Okawa H., Shibata M., Taniguchi K., 2015, *Phys. Rev. D*, **92**, 044028
- Li R., Ho L. C., Ricci C., Trakhtenbrot B., Arcavi I., Kara E., Hiramatsu D., 2022a, *ApJ*, **933**, 70
- Li J., Lai D., Rodet L., 2022b, *ApJ*, **934**, 154
- Linial I., Metzger B. D., 2023, arXiv e-prints, p. arXiv:2303.16231
- Lucchetta G., Ackermann M., Berge D., Bühler R., 2022, *J. Cosmology Astropart. Phys.*, **2022**, 013
- Luo Y., Wu X.-J., Zhang S.-R., Wang J.-M., Ho L. C., Yuan Y.-F., 2023, Monthly Notices of the Royal Astronomical Society, p. stad2188
- MacLeod M., Guillochon J., Ramirez-Ruiz E., Kasen D., Rosswog S., 2016, *ApJ*, **819**, 3
- Maiolino R., Mannucci F., 2019, *A&ARv*, **27**, 3
- Maod D., Mannucci F., Nelemans G., 2014, *ARA&A*, **52**, 107
- Mazzali P. A., Nomoto K., Cappellaro E., Nakamura T., Umeda H., Iwamoto K., 2001, *The Astrophysical Journal*, **547**, 988
- McCutcheon C., Zeng Y., Liu Z. W., Izzard R. G., Pan K. C., Chen H. L., Han Z., 2022, *MNRAS*, **514**, 4078
- McKernan B., Ford K. E. S., Lyra W., Perets H. B., 2012, *MNRAS*, **425**, 460
- McKernan B., Ford K. E. S., Kocsis B., Lyra W., Winter L. M., 2014, *MNRAS*, **441**, 900
- McKernan B., Ford K. E. S., O’Shaughnessy R., 2020, *MNRAS*, **498**, 4088
- McKernan B., Ford K. E. S., Cantiello M., Graham M., Jermyn A. S., Leigh N. W. C., Ryu T., Stern D., 2022, *MNRAS*, **514**, 4102
- Meegan C., et al., 2009, *ApJ*, **702**, 791
- Mészáros P., Rees M. J., 1997, *ApJ*, **476**, 232
- Moiseev A. A., et al., 2015, arXiv e-prints, p. arXiv:1508.07349
- Moranchel-Basurto A., Sánchez-Salcedo F. J., Chametla R. O., Velázquez P. F., 2021, *The Astrophysical Journal*, **906**, 15
- Nagao T., Maiolino R., Marconi A., 2006, *A&A*, **447**, 863
- Nakar E., Sari R., 2010, *ApJ*, **725**, 904
- Orlando E., et al., 2022, *J. Cosmology Astropart. Phys.*, **2022**, 036
- Ostriker J. P., 1983, *ApJ*, **273**, 99
- Pan Z., Yang H., 2021a, *Phys. Rev. D*, **103**, 103018
- Pan Z., Yang H., 2021b, *ApJ*, **923**, 173
- Papenfort L. J., Gold R., Rezzolla L., 2018, *Phys. Rev. D*, **98**, 104028
- Pelassa V., Preece R., Piron F., Omodei N., Guiriec S., 2010, arXiv e-prints, p. arXiv:1002.2617
- Peng P., Chen X., 2021, *MNRAS*, **505**, 1324
- Pereira R., et al., 2013, *A&A*, **554**, A27
- Perets H. B., Li Z., Lombardi James C. J., Milcarek Stephen R. J., 2016, *ApJ*, **823**, 113
- Perlmutter S., et al., 1999, *ApJ*, **517**, 565
- Perna R., Lazzati D., Cantiello M., 2021, *ApJL*, **906**, L7
- Piran T., 1999, *Phys. Rep.*, **314**, 575
- Piro A. L., Morozova V. S., 2016, *ApJ*, **826**, 96
- Radice D., Galeazzi F., Lippuner J., Roberts L. F., Ott C. D., Rezzolla L., 2016, *MNRAS*, **460**, 3255
- Raskin C., Timmes F. X., Scannapieco E., Diehl S., Fryer C., 2009, *MNRAS*, **399**, L156
- Rees M. J., Meszaros P., 1994, *ApJ*, **430**, L93
- Ricci C., et al., 2020, *ApJ*, **898**, L1
- Riess A. G., et al., 1998, *AJ*, **116**, 1009
- Rosswog S., Kasen D., Guillochon J., Ramirez-Ruiz E., 2009, *ApJ*, **705**, L128
- Rowan C., Boekholt T., Kocsis B., Haiman Z., 2022, arXiv e-prints, p. arXiv:2212.06133
- Rozyczka M., Bodenheimer P., Lin D. N. C., 1995, *MNRAS*, **276**, 597
- Rybicki G. B., Lightman A. P., 1991, Radiative processes in astrophysics. John Wiley & Sons
- Samsing J., et al., 2022, *Nature*, **603**, 237
- Schmidt B. P., et al., 1998, *ApJ*, **507**, 46
- Secunda A., Bellovary J., Mac Low M.-M., Ford K. E. S., McKernan B., Leigh N. W. C., Lyra W., Sándor Z., 2019, *ApJ*, **878**, 85
- Shankar F., Weinberg D. H., Miralda-Escudé J., 2009, *ApJ*, **690**, 20
- Shin J., Woo J.-H., Nagao T., Kim S. C., 2013, *ApJ*, **763**, 58
- Shy D., et al., 2022, in den Herder J.-W. A., Nikzad S., Nakazawa K., eds, Society of Photo-Optical Instrumentation Engineers (SPIE) Conference Series Vol. 12181, Society of Photo-Optical Instrumentation Engineers (SPIE) Conference Series. p. 121812G (arXiv:2210.02962), doi:10.1117/12.2628811
- Sirko E., Goodman J., 2003, *MNRAS*, **341**, 501
- Stone N. C., Metzger B. D., Haiman Z., 2017, *MNRAS*, **464**, 946
- Syer D., Clarke C. J., Rees M. J., 1991, *MNRAS*, **250**, 505
- Taam R. E., 1980, *ApJ*, **242**, 749
- Tagawa H., Haiman Z., Kocsis B., 2020, *ApJ*, **898**, 25
- Tanaka H., Takeuchi T., Ward W. R., 2002, *The Astrophysical Journal*, **565**, 1257
- Thompson T. A., Quataert E., Murray N., 2005, *ApJ*, **630**, 167
- Tomsick J., COSI Collaboration 2022, in 37th International Cosmic Ray Conference. p. 652 (arXiv:2109.10403), doi:10.22323/1.395.0652
- Trakhtenbrot B., et al., 2019, *ApJ*, **883**, 94
- Vick M., Lai D., 2019, *Phys. Rev. D*, **100**, 063001
- Vijaykumar A., Kapadia S. J., Ajith P., 2022, *MNRAS*, **513**, 3577
- Wang B., Han Z., 2012, *New Astron. Rev.*, **56**, 122
- Wang J.-S., Lai D., 2020, *Phys. Rev. D*, **102**, 083005
- Wang J.-M., Liu J.-R., Ho L. C., Du P., 2021a, *ApJ*, **911**, L14
- Wang J.-M., Liu J.-R., Ho L. C., Li Y.-R., Du P., 2021b, *ApJ*, **916**, L17



- Warner C., Hamann F., Dietrich M., 2003, *ApJ*, 596, 72
- Webbink R. F., 1984, *ApJ*, 277, 355
- Whelan J., Iben Icko J., 1973, *ApJ*, 186, 1007
- Wilson J. R., Mathews G. J., 2004, *ApJ*, 610, 368
- Yang Y., et al., 2019a, *Phys. Rev. Lett.*, 123, 181101
- Yang Y., Bartos I., Haiman Z., Kocsis B., Márka Z., Stone N. C., Márka S., 2019b, *ApJ*, 876, 122
- Yang Y., Bartos I., Fragione G., Haiman Z., Kowalski M., Marka S., Perna R., Tagawa H., 2021, arXiv e-prints, p. [arXiv:2105.02342](https://arxiv.org/abs/2105.02342)
- Zhu J.-P., Zhang B., Yu Y.-W., Gao H., 2021a, *ApJ*, 906, L11
- Zhu J.-P., Yang Y.-P., Zhang B., Liu L.-D., Yu Y.-W., Gao H., 2021b, *ApJ*, 914, L19
- de Angelis A., et al., 2018, *Journal of High Energy Astrophysics*, 19, 1

This paper has been typeset from a  $\text{\TeX}/\text{\LaTeX}$  file prepared by the author.